A Comparative Study of Passivity Enforcement Schemes for Linear Lumped Macromodels

Stefano Grivet-Talocia, *Senior Member, IEEE*, and Andrea Ubolli

***Abstract*—This paper presents a comparative study of several passivity enforcement schemes for linear lumped macromodels. We consider three main classes of algorithms. First class is represented by those methods based on a direct enforcement of positive/bounded real Lemma constraints via convex optimization. Second class includes those algorithms that enforce the passivity constraints at discrete frequency samples. These schemes are here formulated as second-order cone programs in order to optimize performance. Finally, we consider algorithms based on Hamiltonian eigenvalue perturbation. These three classes are applied to a significant set of benchmark examples, essentially various kinds of high-speed interconnects and packages, with the aim of comparing their performance in terms of accuracy, efficiency, applicability, and robustness. These examples are specifically selected in order to be critical for one or more algorithms, in terms of excessive accuracy degradation, computational complexity, or even lack of convergence. One important result is that carefully designed weighting schemes may dramatically improve performance for all considered algorithm classes.**

***Index Terms*—Bounded real lemma, Hamiltonian matrices, inverse weighting, linear macromodeling, passivity, positive real lemma, second-order cone programming.**

I. Introduction

PASSIVE macromodeling of electrical interconnects, packages, and components has become a common practice in the analysis and design of digital, radio frequency (RF), and mixed signal systems [1], [2]. Macromodeling produces compact behavioral equivalents starting from field simulation results or direct measurements, thus enabling fast simulation in both time and frequency domain since early stages of product development. Several algorithms exist for the derivation of macromodels, vector fitting (VF) being the most common choice in its several formulations [3]–[11].

One main difficulty that must be faced during the derivation of a macromodel is passivity enforcement. Since any passive structure or component is unable to generate energy, also the corresponding models should retain this property [12]–[15]. Otherwise, model use in a numerical simulation may be dangerous, since instabilities may occur [17], [18]. Several papers addressing passivity enforcement have been recently published. We can cite direct methods using positive real lemma (PRL) or bounded real lemma (BRL) [15] constraints [19]–[21], methods for passivity enforcement at discrete frequency samples via linear or quadratic programming [18], [22]–[25], and Hamiltonian-based techniques [17], [26], [27]. Variants of the above schemes have been presented in [28]–[32].

Our main objective is to select the most commonly used algorithms and compare their performance on a set of significant and challenging examples. To this end, an implementation of these schemes on a common platform has been realized. This will enable, in Section V, to draw some general conclusions in terms of accuracy, robustness, and computational requirements. One of the main conclusions is that the performance of all algorithms can be dramatically improved if suitable frequency-selective weighting schemes are employed [30]–[32]. These include inverse weighting for relative error preservation and low-pass weighting for off-band passivity control.

This paper is organized as follows. Section II introduces the basic notation and states the main problem. Section III briefly reviews the considered passivity enforcement schemes, describing the particular implementation that we use for our comparison. Section IV presents the weighting schemes that we use to optimize performance. Finally, Section V applies the various techniques to a set of benchmark examples and presents the results. Main conclusions are drawn in Section VI.

II. Preliminaries and Notation

Throughout this paper x, $\boldsymbol{x}$, and $\boldsymbol{X}$ denote a generic scalar, vector (lowercase and boldface), and matrix (uppercase and boldface), respectively. Superscripts *, ^{T}, and ^{H} are used for the complex conjugate, transpose, and conjugate (Hermitian) transpose, respectively. Operator $\otimes$ denotes the Kronecker matrix product [33], [34], $\mathrm{vec}\{\boldsymbol{X}\}$ stacks the columns of $\boldsymbol{X}$ in a single column vector, and $\mathrm{tr}\{\boldsymbol{X}\}$ is the matrix trace. We will use $\lambda\{\boldsymbol{X}\}$ and $\sigma\{\boldsymbol{X}\}$ to denote the set of eigenvalues and singular values of $\boldsymbol{X}$, respectively. The matrix 2-norm will be denoted as $\|\boldsymbol{X}\|_2 = \max\sigma\{\boldsymbol{X}\}$.

We consider linear macromodels in state-space form, described by the following standard shorthand notation [35]:

$$\boldsymbol{H}(s) = \boldsymbol{D} + \boldsymbol{C}(s\boldsymbol{I} - \boldsymbol{A})^{-1}\boldsymbol{B} \leftrightarrow \left[\begin{array}{c|c} \boldsymbol{A} & \boldsymbol{B} \\ \hline \boldsymbol{C} & \boldsymbol{D} \end{array}\right] \tag{1}$$

where s is the Laplace variable, $\boldsymbol{H}(s)$ is the $p \times p$ transfer matrix of the macromodel, and $\{\boldsymbol{A}, \boldsymbol{B}, \boldsymbol{C}, \boldsymbol{D}\}$ are the state-space matrices of some realization associated to $\boldsymbol{H}(s)$. We will assume a strictly stable macromodel, with all n eigenvalues of $\boldsymbol{A}$ confined in the region $\mathbb{R}\mathrm{e}\{s\} < 0$. Both scattering and hybrid

Manuscript received October 17, 2007; revised January 24, 2008. First published May 28, 2008; current version published November 28, 2008. This work was recommended for publication by Associate Editor F. Canavero upon evaluation of the reviewers comments.

The authors are with the Department of Electronics, Politecnico di Torino, Torino 10129, Italy (e-mail: stefano.grivet@polito.it; andrea.ubolli@polito.it).

Color versions of one or more of the figures in this paper are available online at http://ieeexplore.ieee.org.

Digital Object Identifier 10.1109/TADVP.2008.926004

(including admittance and impedance) input–output representations will be considered, for the sake of generality. A unified formulation will be obtained by defining

$$\boldsymbol{\Phi}(s) = \begin{cases} \boldsymbol{H}^H(s) + \boldsymbol{H}(s), & \text{hybrid case} \\ \boldsymbol{I} - \boldsymbol{H}^H(s), \boldsymbol{H}(s) & \text{scattering case} \end{cases}. \quad (2)$$

The model in (1) is passive when the following conditions are fulfilled [12]–[15]:

1) $\boldsymbol{H}(s)$ is defined and analytic in $\mathbb{R}\mathrm{e}\{s\} > 0$;
2) $\boldsymbol{\Phi}(s) \geq 0; \forall s : \mathbb{R}\mathrm{e}\{s\} > 0$
3) $\boldsymbol{H}(s^*) = \boldsymbol{H}^*(s)$.

Note that for scattering representations no poles are allowed on the imaginary axis [16], and condition 1) must hold for $\mathbb{R}\mathrm{e}\{s\} \geq 0$. This is guaranteed by the working assumption of strict stability.

Conditions 1) and 3) are guaranteed by most macromodeling schemes. Conversely, fulfillment of condition 2) poses serious numerical challenges. This fact motivated significant research efforts during the last few years, aimed at the definition of fast and robust algorithms for model passivity enforcement. Section III reviews some of these algorithms and describes their particular implementation that we employ in this work in order to compare their performance.

III. Passivity Enforcement Schemes

The various passivity enforcement schemes that we compare in this paper are briefly described in the following subsections. Namely, our implementation of PRL/BRL constraints is outlined in Section III-A. We introduce in Section III-B a second-order-cone programming scheme allowing for passivity enforcement at discrete frequency samples, leading to global passivity via iterative application. Finally, we recall the main steps of recently introduced Hamiltonian perturbation schemes in Section III-C.

Unless otherwise noted, the generic passivity enforcement scheme computes a perturbation in the model coefficients, so that the perturbed model is passive. In this work, we concentrate on a perturbation of the single state-space matrix

$$\widehat{\boldsymbol{C}} = \boldsymbol{C} + \boldsymbol{\Delta} \quad (3)$$

which typically stores the residue matrices of the macromodel. In case the model is not asymptotically passive for $s \to \infty$, a direct correction of the direct coupling term $\boldsymbol{D}$ can be applied in a preprocessing stage, following the procedure of [17] and [22]. The same consideration applies to improper macromodels in hybrid form that include a linear term $s\boldsymbol{E}$, which is not considered in this work.

The perturbation (3) corresponds to a total of np scalar unknowns. All considered schemes find a perturbation term $\boldsymbol{\Delta}$ such that the new model is passive, with the accuracy constraint

$$\min \|\boldsymbol{\Delta}\|. \quad (4)$$

Throughout this section, a generic norm will be used to present the various schemes, since different norms lead to different performance. Various alternatives will be detailed and commented in Section IV.

A. PRL/BRL

The PRL

$$\begin{bmatrix} -\boldsymbol{A}^T\boldsymbol{P} - \boldsymbol{P}\boldsymbol{A} & -\boldsymbol{P}\boldsymbol{B} + \boldsymbol{C}^T \\ -\boldsymbol{B}^T\boldsymbol{P} + \boldsymbol{C} & \boldsymbol{D} + \boldsymbol{D}^T \end{bmatrix} \geq 0 \quad (5)$$

with $\boldsymbol{P} = \boldsymbol{P}^T > 0$, and the BRL

$$\begin{bmatrix} \boldsymbol{A}^T\boldsymbol{P} + \boldsymbol{P}\boldsymbol{A} & \boldsymbol{P}\boldsymbol{B} & \boldsymbol{C}^T \\ \boldsymbol{B}^T\boldsymbol{P} & -\boldsymbol{I} & \boldsymbol{D}^T \\ \boldsymbol{C} & \boldsymbol{D} & -\boldsymbol{I} \end{bmatrix} \leq 0 \quad (6)$$

with $\boldsymbol{P} = \boldsymbol{P}^T > 0$, are fully equivalent formulations of the passivity constraints 1)–3) of Section II for hybrid and scattering representations, respectively [15], [35]. The main advantage of PRL and BRL is the purely algebraic formulation as a linear matrix inequality (LMI), which is a convex formulation. Hence, the direct enforcement of such constraints admits an optimal and unique solution, which can be achieved in a finite number of iterations within any prescribed tolerance [36].

Several formulations available in the literature [19]–[21] perform a parameterization of the matrix $\boldsymbol{P}$ in order to avoid the constraint on its positive definiteness and to reduce the computational requirements for the numerical solution. We follow this strategy also in this work, by rewriting PRL and BRL in block-matrix form, respectively, as

$$\boldsymbol{\Psi}_P = \boldsymbol{\Psi}_P^T = \begin{bmatrix} \boldsymbol{\Psi}_P^{11} & \boldsymbol{\Psi}_P^{12} \\ \left(\boldsymbol{\Psi}_P^{12}\right)^T & \boldsymbol{\Psi}_P^{22} \end{bmatrix} \geq 0 \quad (7)$$

$$\boldsymbol{\Psi}_B(\boldsymbol{C}) = \boldsymbol{\Psi}_B^T(\boldsymbol{C}) = \begin{bmatrix} \boldsymbol{\Psi}_B^{11} & \boldsymbol{\Psi}_B^{12} & \boldsymbol{C}^T \\ \left(\boldsymbol{\Psi}_B^{12}\right)^T & -\boldsymbol{I} & \boldsymbol{D}^T \\ \boldsymbol{C} & \boldsymbol{D} & -\boldsymbol{I} \end{bmatrix} \leq 0. \quad (8)$$

In the PRL case (7), we can relate the blocks $\boldsymbol{\Psi}_P^{12}$ and $\boldsymbol{\Psi}_P^{11}$, since it can be proved [19]–[21] that

$$(\boldsymbol{P}\boldsymbol{B})_{ij} = \mathrm{tr}\left\{\boldsymbol{\zeta}_{ij}\boldsymbol{\Psi}_P^{11}\right\} = \boldsymbol{\varepsilon}_{ij}^T \mathrm{vec}\left\{\boldsymbol{\Psi}_P^{11}\right\} \quad (9)$$

for $i = 1, \ldots, n$ and $j = 1, \ldots, p$, with

$$\boldsymbol{\varepsilon}_{ij} = \mathrm{vec}\left\{\boldsymbol{\zeta}_{ij}^T\right\} \quad (10)$$

and where matrix $\boldsymbol{\zeta}_{ij}$ is found [19] as the solution of a suitably-defined Lyapunov equation. As a result, the PRL constraints are restated for our problem as

$$\begin{cases} \min \|\boldsymbol{\Delta}\| \\ C_{ji} + \Delta_{ji} = \boldsymbol{\varepsilon}_{ij}^T \mathrm{ve}\left\{\boldsymbol{\Psi}_P^{11}\right\} + \left(\boldsymbol{\Psi}_P^{12}\right)_{ij} \\ \boldsymbol{\Psi}_P \geq 0 \end{cases}. \quad (11)$$

The same procedure, applied to the BRL case (8) leads to

$$\begin{cases} \min \|\boldsymbol{\Delta}\| \\ \left(\boldsymbol{\Psi}_B^{12}\right)_{ij} = \boldsymbol{\varepsilon}_{ij}^T \mathrm{vec}\left\{\boldsymbol{\Psi}_B^{11}\right\} . \\ \boldsymbol{\Psi}_B(\boldsymbol{C}+\boldsymbol{\Delta}) \le 0 \end{cases} \tag{12}$$

The above schemes can be easily modified in order to minimize the model deviation with respect to the frequency samples (total K in the following) of the raw data $\widetilde{\boldsymbol{H}}(j\omega_k)$ from which the macromodel was constructed in first place, instead of minimizing the deviation between perturbed and original macromodel. To this end, the first row in (11), (12) is replaced by

$$\min t : \left\| \mathrm{vec}\left\{ \boldsymbol{H}(j\omega) - \widetilde{\boldsymbol{H}}(j\omega) \right\} \right\|_2 < t \tag{13}$$

where t is a slack variable. All formulations (11)–(13) can be solved via convex optimization using one of the several available solvers. In this work, we employ SeDuMi [37], [38] as the optimization engine, in combination with the YALMIP driver [39] for the MATLAB [40] environment.

B. Enforcing Passivity at Discrete Frequencies

A second class of passivity enforcement schemes is based on the direct enforcement of the passivity constraints at few carefully selected frequency samples. This is possible thanks to the strict stability assumption on the macromodel, which allows to restate the condition 2) of Section II as

$$\min \lambda \left\{ \boldsymbol{\Phi}(j\omega) \right\} \ge 0, \quad \forall \omega. \tag{14}$$

This condition is checked at a suitably defined set of discrete frequency points. If some frequencies are found that violate (14), the perturbation (3) is applied to the macromodel, with the aim of removing all passivity violations and recover global passivity.

There are several possible implementations [18], [22]–[25], differing on the choice of the frequency samples and on the form of the constraint (14) that is employed in the optimization loop. In this work, we consider a projection-based perturbation, that is able to displace any individual eigenvalue exceeding the critical threshold 0, at all frequencies that correspond to a local negative minimum of the eigenvalue trajectories. The total number of these eigenvalues will be denoted as m in the following.

We start by considering a single frequency ω_0 at which condition (14) is violated by a negative eigenvalue $\lambda_i < 0$. Let the corresponding eigenvector of $\boldsymbol{\Phi}_0 = \boldsymbol{\Phi}(j\omega_0)$ be $\boldsymbol{v}_i$, normalized such that $\|\boldsymbol{v}_i\|_2 = 1$. A first-order eigenvalue perturbation analysis [41] applied to $\boldsymbol{\Phi}_0$ leads to

$$\widehat{\lambda}_i \simeq \lambda^i + \boldsymbol{v}_i^H (\boldsymbol{\delta\Phi}_0) \boldsymbol{v}_i \tag{15}$$

where $\boldsymbol{\delta\Phi}_0$ is the matrix perturbation that is required to displace λ_i to the new location $\widehat{\lambda}_i$. A few straightforward algebraic manipulations allow to relate this matrix perturbation to the model perturbation $\boldsymbol{\Delta}$. The result is

$$\widehat{\lambda}_i \simeq \lambda^i + \boldsymbol{w}_i \mathrm{vec}\{\boldsymbol{\Delta}\} \tag{16}$$

where the row-vector $\boldsymbol{w}_i$ is defined as

$$\boldsymbol{w}_i = -2\mathbb{R}\mathrm{e}\left\{ (\boldsymbol{K}_0 \boldsymbol{v_i})^T \otimes (\boldsymbol{H}_0 \boldsymbol{v_i})^H \right\} \tag{17}$$

in the scattering case and

$$\boldsymbol{w}_i = 2\mathbb{R}\mathrm{e}\left\{ (\boldsymbol{K}_0 \boldsymbol{v_i})^T \otimes (\boldsymbol{v_i})^H \right\} \tag{18}$$

in the hybrid case, with

$$\boldsymbol{K}_0 = (j\omega_0 \boldsymbol{I} - \boldsymbol{A})^{-1} \boldsymbol{B} \tag{19}$$

and

$$\boldsymbol{H}_0 = \boldsymbol{H}(j\omega_0) = \boldsymbol{D} + \boldsymbol{C}\boldsymbol{K}_0. \tag{20}$$

Enforcing now $\widehat{\lambda}_i \ge 0$ leads to the following linear inequality constraint

$$\boldsymbol{w}_i \mathrm{vec}\{\boldsymbol{\Delta}\} \ge -\lambda_i \tag{21}$$

valid for both scattering and hybrid formulations. In the scattering case, we also consider the additional constraint

$$\boldsymbol{w}_i \mathrm{vec}\{\boldsymbol{\Delta}\} \le 1 - \lambda_i \tag{22}$$

since the eigenvalues of $\boldsymbol{\Phi}_0$ must also be bounded by one.

The above constraints are collected and formulated as a second-order cone program (SOCP)

$$\begin{cases} \min t \\ \|\boldsymbol{\Delta}\| < t \\ \boldsymbol{W}\mathrm{vec}\{\boldsymbol{\Delta}\} \ge \boldsymbol{b} \end{cases} \tag{23}$$

where t is a slack variable, the first constraint defines a cone in the embedding vector space, and the last constraint collects (21), (22) for all m eigenvalues to be perturbed. We adopt this formulation since very efficient solvers exist for SOCP optimization. In this work, we use the SeDuMi optimization engine [37], [38].

The above scheme enforces local passivity only at discrete frequency points and is thus unable to guarantee global passivity. Therefore, we embed the above SOCP into an outer iterative process. At each iteration, an adaptive sampling [27] of the frequency-dependent eigenvalues $\boldsymbol{\Phi}(j\omega)$ is performed, and passivity is enforced using (23) at the frequency samples where the largest violations are found. Global passivity is usually achieved in few iterations, as documented in Section V-G.

C. Hamiltonian Perturbation Schemes

The third class of global passivity enforcement schemes that we consider is based on the iterative perturbation of Hamiltonian matrices [17], [26], [27]. These matrices are defined as

$$\mathcal{N}_\alpha = \begin{bmatrix} \boldsymbol{A} + \boldsymbol{B}\boldsymbol{Q}_\alpha^{-1}\boldsymbol{C} & \boldsymbol{B}\boldsymbol{Q}_\alpha^{-1}\boldsymbol{B}^T \\ -\boldsymbol{C}^T\boldsymbol{Q}_\alpha^{-1}\boldsymbol{C} & -\boldsymbol{A}^T - \boldsymbol{C}^T\boldsymbol{Q}_\alpha^{-1}\boldsymbol{B}^T \end{bmatrix} \tag{24}$$

with $\boldsymbol{Q}_\alpha = (2\alpha\boldsymbol{I} - \boldsymbol{D} - \boldsymbol{D}^T)$, for hybrid representations, and

$$\mathcal{M}_\gamma = \begin{bmatrix} \boldsymbol{A} - \boldsymbol{B}\boldsymbol{R}_\gamma^{-1}\boldsymbol{D}^T\boldsymbol{C} & -\gamma\boldsymbol{B}\boldsymbol{R}_\gamma^{-1}\boldsymbol{B}^T \\ \gamma\boldsymbol{C}^T\boldsymbol{S}_\gamma^{-1}\boldsymbol{C} & -\boldsymbol{A}^T + \boldsymbol{C}^T\boldsymbol{D}\boldsymbol{R}_\gamma^{-1}\boldsymbol{B}^T \end{bmatrix} \tag{25}$$

with $\boldsymbol{R}_\gamma = (\boldsymbol{D}^T\boldsymbol{D} - \gamma^2\boldsymbol{I})$ and $\boldsymbol{S}_\gamma = (\boldsymbol{D}\boldsymbol{D}^T - \gamma^2\boldsymbol{I})$ for scattering representations. It can be shown that under suitable tech-

nical assumptions [15], [26], [42], the model (1) is not passive when the set $\{\omega_i\}$ of (simple) purely imaginary eigenvalues of $\mathcal{N}_0$ (hybrid) or $\mathcal{M}_1$ (scattering) is nonempty. We remark that the above Hamiltonian matrices are constant (frequency-independent), so that the determination of all (imaginary) eigenvalues provides a global passivity characterization, without requiring any frequency sampling process.

The derivation in [26] shows that passivity is achieved by iterative first-order perturbation of such eigenvalues $\{\omega_i\}$. This can be expressed as a linear constraint as

$$\mathbb{R}\mathrm{e}\left\{\boldsymbol{v}_{i1}^T \otimes \boldsymbol{z}_i^H\right\} \mathrm{vec}\{\boldsymbol{\Delta}\} = \mathbb{I}\mathrm{m}\left\{\boldsymbol{v}_{i1}^H \boldsymbol{v}_{i2}\right\} \delta\omega_i \tag{26}$$

where $\delta\omega_i$ denotes the desired perturbation on the ith imaginary eigenvalue, and

$$\boldsymbol{v}_i = \begin{bmatrix} \boldsymbol{v}_{i1} \\ \boldsymbol{v}_{i2} \end{bmatrix} \tag{27}$$

is the right eigenvector of the Hamiltonian matrix associated to the eigenvalue ω_i. The auxiliary vector $\boldsymbol{z}_i$ is defined as

$$\boldsymbol{z}_i = -\boldsymbol{Q}_0^{-1}\boldsymbol{B}^T\boldsymbol{v}_{i2} - \boldsymbol{Q}_0^{-1}\boldsymbol{C}\boldsymbol{v}_{i1} \tag{28}$$

in the hybrid case and

$$\boldsymbol{z}_i = \boldsymbol{D}\boldsymbol{R}_1^{-1}\boldsymbol{B}^T\boldsymbol{v}_{i2} + \boldsymbol{S}_1^{-1}\boldsymbol{C}\boldsymbol{v}_{i1} \tag{29}$$

in the scattering case. Collecting all constraints leads to the following optimization problem:

$$\begin{cases} \min \|\boldsymbol{\Delta}\| \\ \boldsymbol{Z}\mathrm{vec}\{\boldsymbol{\Delta}\} = \boldsymbol{y} \end{cases}. \tag{30}$$

The above formulation is not convex. This implies that an iterative application of (30) may fail to converge. This is indeed quite common when $\|\boldsymbol{D}\|_2 \simeq 1$ (for scattering representations) and $\boldsymbol{D} + \boldsymbol{D}^T$ is nearly singular (for hybrid representations). In such cases, the Hamiltonian eigenvalue perturbation becomes ill-conditioned, as can be easily noted from (24) and (25). Another drawback, mainly in terms of computational complexity, is the requirement of extracting all imaginary eigenvalues of the Hamiltonian matrix in order to write (30). Some techniques for speeding up this operation and potentially allowing for nearly linear complexity are documented in [17] and [27] and are exploited in our implementation. On the other hand, the very limited number of equality constraints (one for each imaginary Hamiltonian eigenvalue, n_i in the following), allows for the numerical solution using standard pseudoinverse methods [40] in negligible time.

IV. Accuracy Preservation and Weighting Schemes

All passivity enforcement schemes presented in Section III are complemented by the accuracy control condition (4). In this section, we present various alternative definitions of this norm, which lead to dramatically different performances.

The standard choice is to minimize the global energy (squared $\mathcal{L}^2$-norm) in the model perturbation $\delta\boldsymbol{H}$, which can be expressed as

$$\|\boldsymbol{\Delta}\|_A^2 = \|\delta\boldsymbol{H}\|_{\mathcal{L}^2}^2 = \frac{1}{2\pi}\sum_{ik}\int_{-\infty}^{\infty} |\delta H_{ik}(j\omega)|^2 \,\mathrm{d}\omega = \mathrm{tr}\{\boldsymbol{\Delta}\boldsymbol{P}_c\boldsymbol{\Delta}^T\} \tag{31}$$

where $\boldsymbol{P}_c$ is the controllability Gramian [13] associated to (1). The main advantage of this definition is the purely algebraic characterization of the norm in terms of the state-space perturbation $\boldsymbol{\Delta}$, which allows a direct use of (31) within all presented schemes (11), (12), (23), and (30).

The major drawback of norm (31) is evident from its definition. This norm provides an absolute error metric over the entire frequency axis. However, we are only interested in the model responses within the modeling bandwidth, say $\omega \in [0, \Omega]$. The off-band behavior of the model is not relevant, as far as the final model is guaranteed to be globally passive. Consequently, a bandlimited accuracy metric is more desirable. This can be achieved as

$$\begin{aligned} \|\boldsymbol{\Delta}\|_W^2 &= \frac{1}{2\pi}\sum_{ik}\int_{-\Omega}^{\Omega} |\delta H_{ik}(j\omega)|^2 \,\mathrm{d}\omega \\ &\simeq \frac{1}{2\pi}\sum_{ik}\int_{-\infty}^{\infty} |W_{ik}(j\omega)\delta H_{ik}(j\omega)|^2 \,\mathrm{d}\omega \\ &= \mathrm{tr}\left\{\boldsymbol{\Delta}\boldsymbol{P}_c^w\boldsymbol{\Delta}^T\right\} \end{aligned} \tag{32}$$

where $W_{ik}(s)$ is the frequency response of a lowpass filter with a sharp cutoff at $\omega = \Omega$. Also this norm has a purely algebraic representation, similar to (31), but employing a modified weighted Gramian $\boldsymbol{P}_c^w$. This matrix is readily computed starting from (1) and from the state-space realization of the filter

$$\boldsymbol{W}(s) \leftrightarrow \left[\begin{array}{c|c} \boldsymbol{A}_w & \boldsymbol{B}_w \\ \hline \boldsymbol{C}_w & \boldsymbol{D}_w \end{array}\right]. \tag{33}$$

The reader is referred to [35], [43], and [44] for basic definitions, and to [31] and [32] for implementation details. In all our tests we used an elliptic filter with in-band ripple less than 0.2 dB and off-band attenuation larger than 40 dB.

The filter $W_{ik}(s)$ can have any arbitrary frequency response, as far as its state-space representation (33) is known. Therefore, is it quite straightforward to adapt (32) so that it represents the (elementwise) relative error instead of the absolute error (31). It is sufficient to define a different weight for each individual transfer matrix element $H_{ik}(s)$

$$W_{ik}(s) = H_{ik}^{-1}(s) \leftrightarrow \left[\begin{array}{c|c} \boldsymbol{A}_{ik} - \boldsymbol{b}_{ik}d_{ik}^{-1}\boldsymbol{c}_{ik} & -\boldsymbol{b}_{ik}d_{ik}^{-1} \\ \hline d_{ik}^{-1}\boldsymbol{c}_{ik} & d_{ik}^{-1} \end{array}\right] \tag{34}$$

where the partial state-space representation matrices $\{\boldsymbol{A}_{ik}, \boldsymbol{b}_{ik}, \boldsymbol{c}_{ik}, d_{ik}\}$ are readily extracted from (1). This inverse weighting is useful for all applications that require relative accuracy preservation over a large dynamic range, including components and packages for RF and mixed-signal applications. See [31] for details.

V. Benchmarks

We now compare the performance of all passivity enforcement schemes applied to several benchmark examples (some of these examples will be made available online[1]). In all cases, a suitable implementation of the VF scheme [11] was used to derive an initial macromodel from raw frequency data. The various passivity enforcement schemes were then applied to this original (nonpassive) macromodel for all benchmarks. Labeling of all results will be consistent in this section, according to the following notation.

RAW	Raw data (frequency samples) used to extract the macromodel in first place.
MOD	Original (nonpassive) macromodel.
BRM	Bounded real constraints, with model error minimization, as in (12).
BRD	Bounded real constraints with data error minimization, as in (13).
SOC	Second-order cone constraints at discrete frequency samples, as in (23).
HAM	Hamiltonian perturbation constraints, as in (30).
−R	This suffix denotes inverse weighting (34) applied in conjunction with any of the above formulations.
−F	This suffix denotes lowpass weighting (32) applied in conjunction with any of the above formulations.

Sections V-A–V-F present the results for each individual benchmark. Section V-G will summarize the computational requirements for all cases.

A. Low-Complexity Package

The first example is a package structure with only $p = 6$ modeled ports, over a 2-GHz bandwidth. Due to the small electrical size, only six poles are needed to fit each response, leading to an overall macromodel dynamic size $n = 36$. The moderate complexity of the macromodel allows application of all techniques presented in Section III. Main difficulty with this example is represented by the very large passivity violation that occurs for frequencies outside the modeled bandwidth. Fig. 1 shows a maximum singular value of the model responses exceeding 2 around 4.2 GHz.

The only method that is able to preserve a good accuracy during passivity enforcement is BRD. All other methods that attempt accuracy preservation with respect to the original nonpassive macromodel fail, as illustrated by Fig. 2. This failure is easily justified, since the standard norm (31) provides a measure of the model perturbation over the entire frequency axis, whereas we are only interested in accuracy preservation up to 2 GHz. Any procedure that minimizes this norm will take into account the model responses beyond 2 GHz. Therefore, the large perturbation required in this case destroys model accuracy at all frequencies during passivity enforcement.

[1]http://www.emc.polito.it/macro

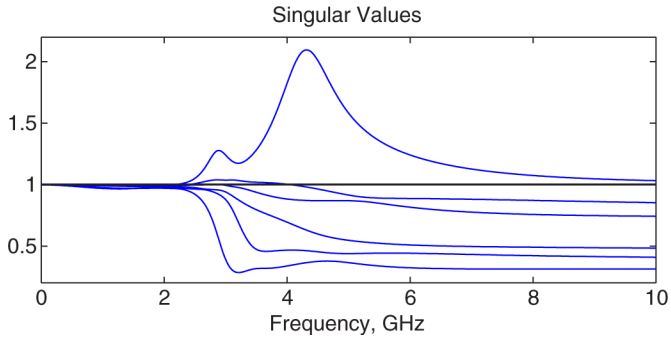

Fig. 1. Singular values of the nonpassive package model of Section V-A.

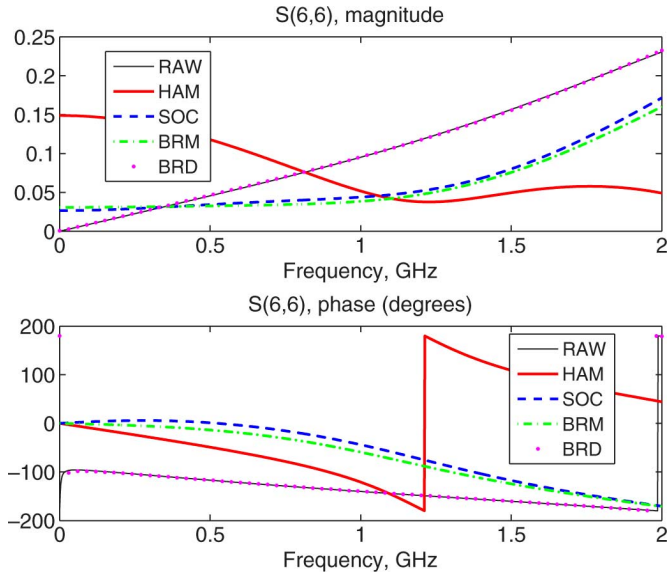

Fig. 2. Responses of various passive models compared to raw scattering data for the package structure of Section V-A.

The situation changes when a suitable lowpass filter is used in the definition of the accuracy metric, as described in Section IV. This lowpass filter reduces dramatically the significance of the model perturbation for off-band frequencies, leading to a behavior similar to BRD. Indeed, Fig. 3 shows that all methods perform equally well, as far as a good lowpass weighting scheme is adopted.

B. Connector

The second example is a large connector, with $p = 18$ modeled ports over a 20-GHz bandwidth. Many poles are required for each element of the scattering matrix, resulting in a macromodel dynamic order $n = 1616$. In this situation, model complexity is far from being tractable with BR-type constraints, mainly due to the excessive number of unknowns in the optimization problems (12) and (13). The passivity violation is moderate, see Fig. 4, showing a peak in some singular value curves slightly outside the modeled bandwidth.

Fig. 5 shows the results obtained with the two applicable schemes, which were run with standard absolute error minimization and no weighting. Accuracy is excellent for all responses, including small crosstalk values such as the scattering response depicted in the plot.

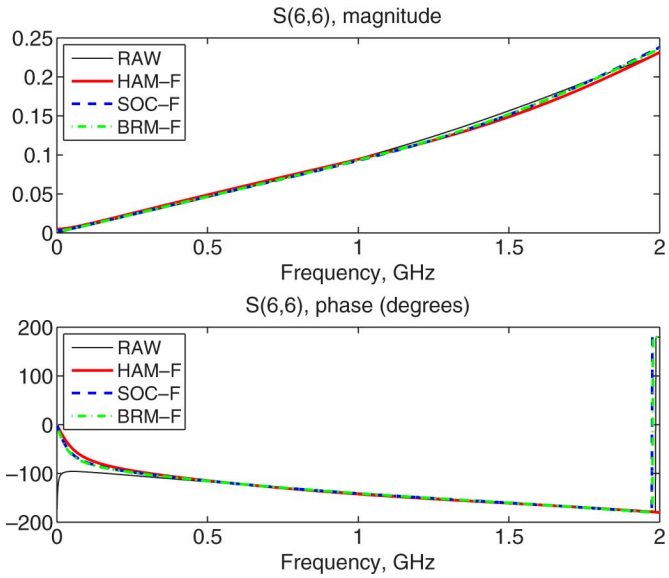

Fig. 3. As in Fig. 2, but employing a lowpass weighted norm during passivity enforcement.

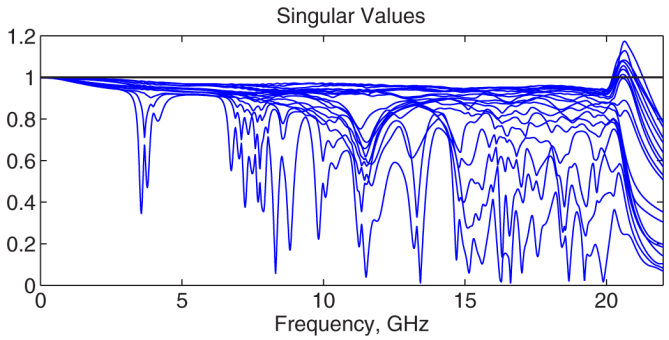

Fig. 4. Singular values of the nonpassive connector model of Section V-B.

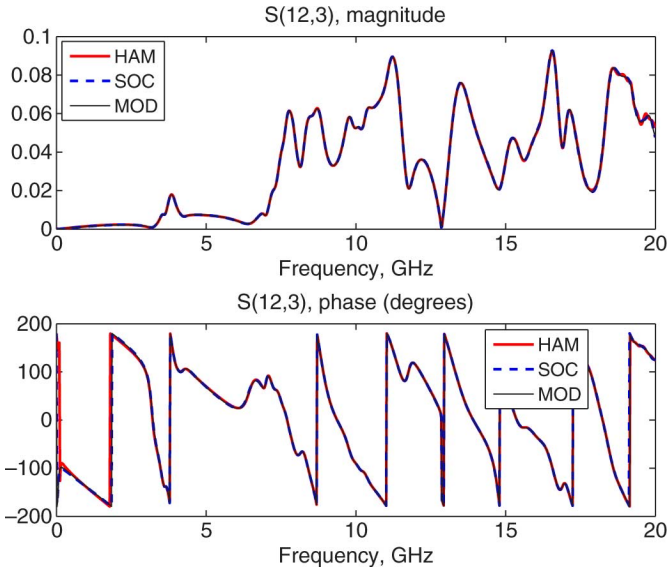

Fig. 5. Responses of various passive models compared to raw scattering data for the connector of Section V-B.

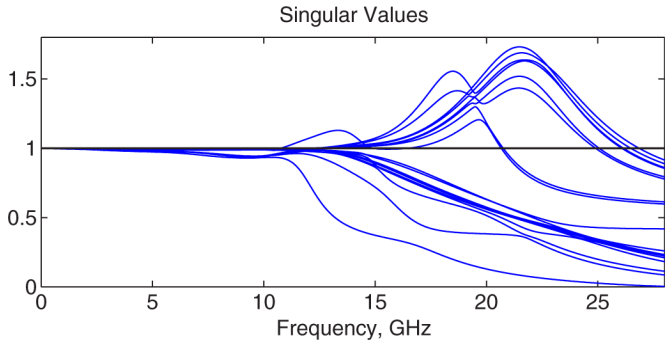

Fig. 6. Singular values of the non-passive via field model of Section V-C.

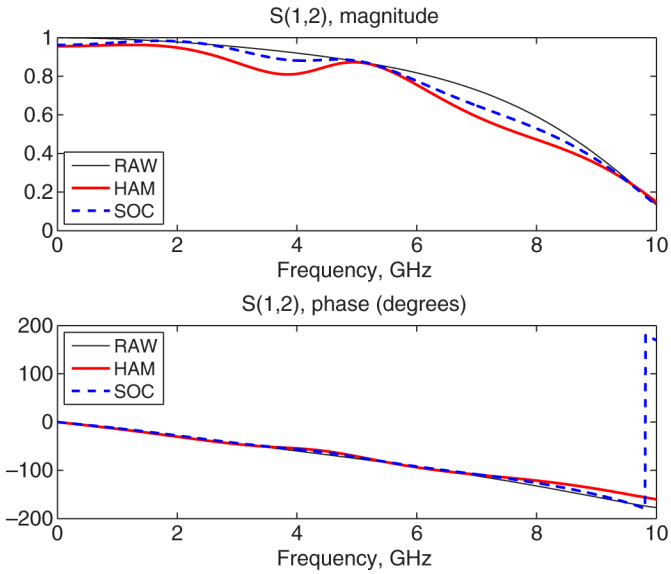

Fig. 7. Responses of various passive models compared to raw scattering data for the via field of Section V-C.

C. Via Field

This example is a via field on a multilayer PCB, with $p = 18$ modeled ports over a 10-GHz bandwidth. As in Section V-A, the moderate electrical size requires few poles for each response, leading to a macromodel dynamic order $n = 216$. Also in this case the passivity violation is quite large, but mainly restricted outside the modeled bandwidth, see Fig. 6. Both BRD and BRM methods failed due to excessive memory requirements in the formulation of the optimization problems (12) and (13).

Fig. 7 shows the results of standard SOC and HAM methods on a transmission coefficient. Accuracy degradation is significant, due to the large perturbation required to reduce the model singular values below one. As for Section V-A, a large off-band passivity violation degrades in-band accuracy, unless a suitable weighting scheme is used. Fig. 8 reports the results obtained with a lowpass filter with cutoff at the edge of the modeled bandwidth. Accuracy is now excellent.

D. Another via Field

This example is another PCB via field, with $p = 18$ modeled ports over a 15-GHz bandwidth, resulting in a macromodel dynamic order $n = 288$. This example introduces an additional difficulty with respect to Section V-C. As depicted in the top

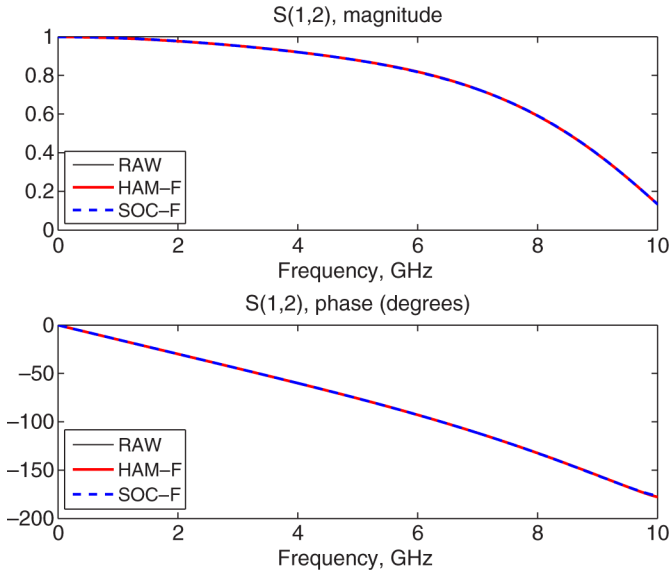

Fig. 8. As in Fig. 7, but employing a lowpass weighted norm during passivity enforcement.

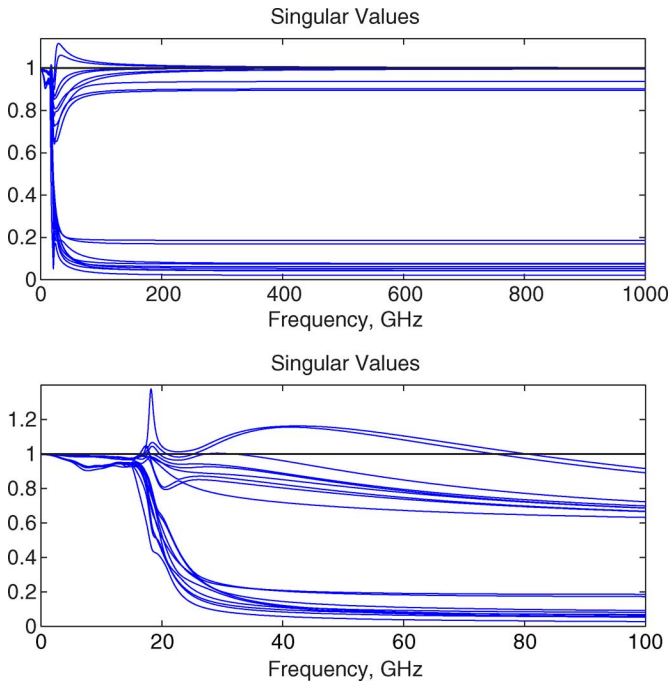

Fig. 9. Singular values of the non-passive via field model of Section V-D. Top panel refers to the unconstrained model, bottom panel refers to the model with an asymptotic hard bound on the singular values, see text.

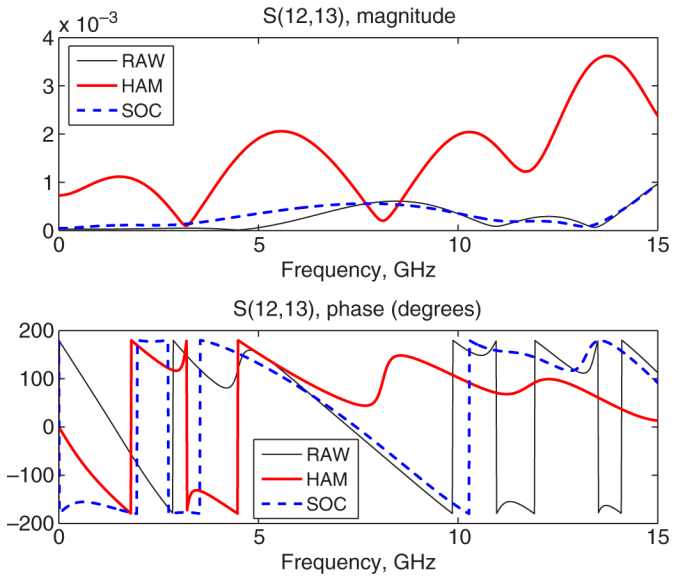

Fig. 10. Responses of various passive models compared to raw scattering data for the via field of Section V-D.

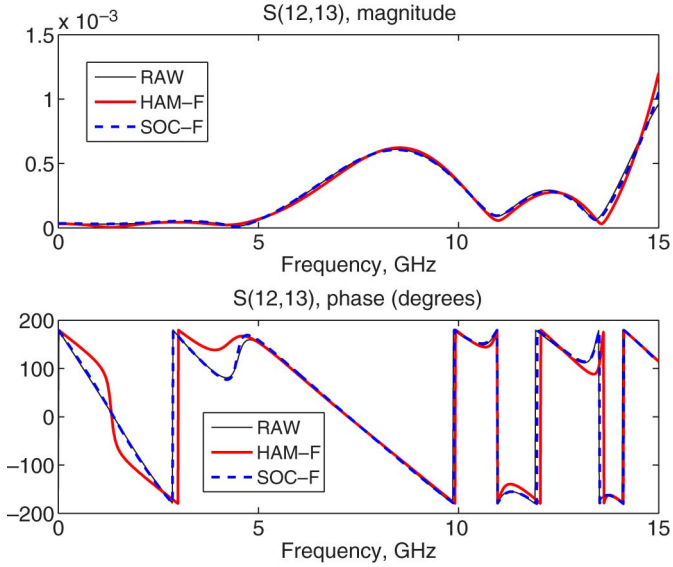

Fig. 11. As in Fig. 10, but employing a lowpass weighted norm during passivity enforcement.

panel of Fig. 9, the high-frequency asymptotic behavior of some singular values approaches one. This was verified by computing $\|\boldsymbol{D}\|_2 = 0.999$. In such cases, the HAM formulation of Section III-C results ill-conditioned, and it is very likely that accuracy is seriously degraded, the number of iterations is too large, or the scheme is even nonconverging. Lack of convergence was indeed the case. In order to improve HAM convergence, a new model was generated by enforcing $\|\boldsymbol{D}\|_2 = 0.6$ as a hard constraint during the computation of poles and residues via VF, using the strategy described in [17]. The particular value to be used for $\|\boldsymbol{D}\|_2$ is not critical, as far as it is not too close to one. The resulting singular values are depicted in the bottom panel of Fig. 9. We remark that in-band model accuracy was comparable in both cases.

Figs. 10 and 11 report the results of HAM and SOC schemes (BRM and BRD were not applicable due to model complexity) applied to this new macromodel without and with lowpass weighting, respectively. As expected, due to the large off-band passivity violations (here both in terms of maximum singular value and width of violation frequency band), the lowpass-filtered implementations outperform the standard schemes.

E. Package With High Dynamic Range

This example illustrates the need of advanced inverse weighting schemes. The structure is a package with $p = 6$

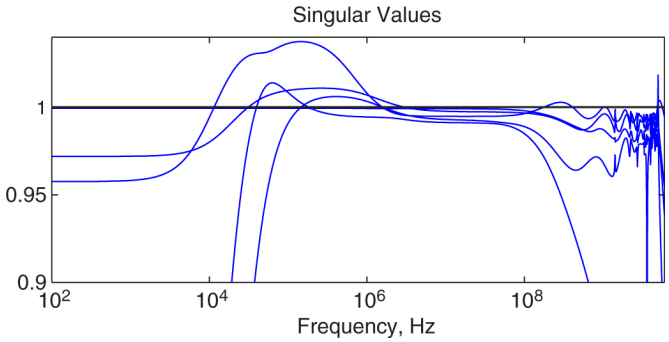

Fig. 12. Singular values of the nonpassive package model of Section V-E.

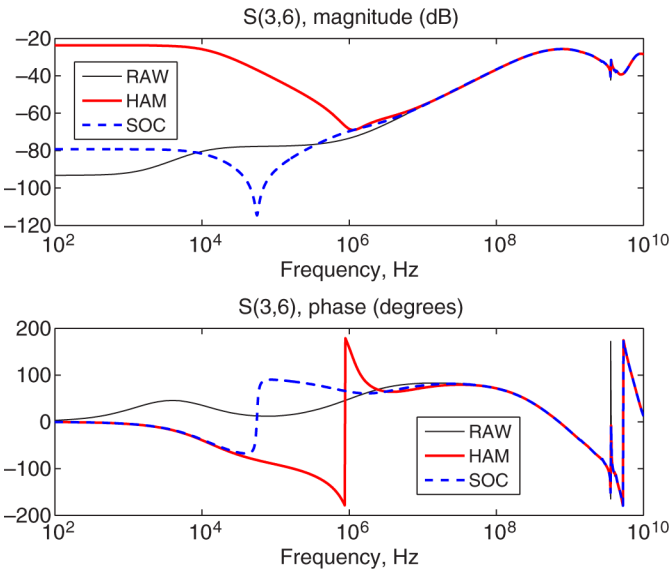

Fig. 13. Responses of various passive models compared to raw scattering data for the via field of Section V-E.

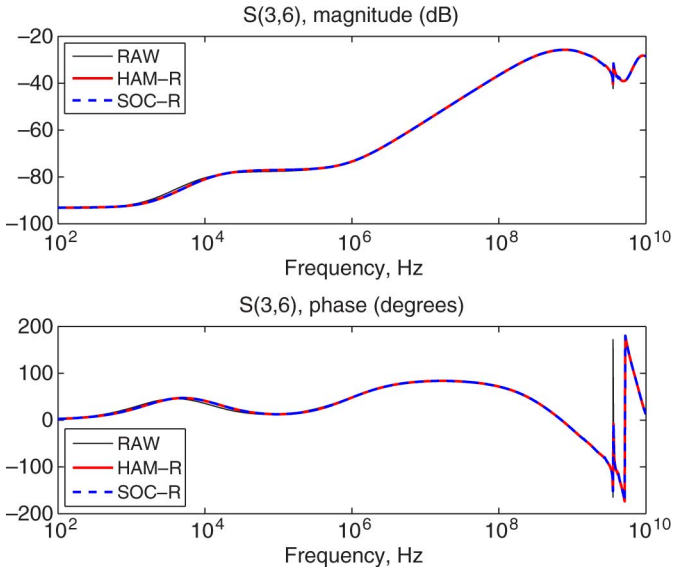

Fig. 14. As in Fig. 13, but employing an inverse weighted norm during passivity enforcement for relative error control.

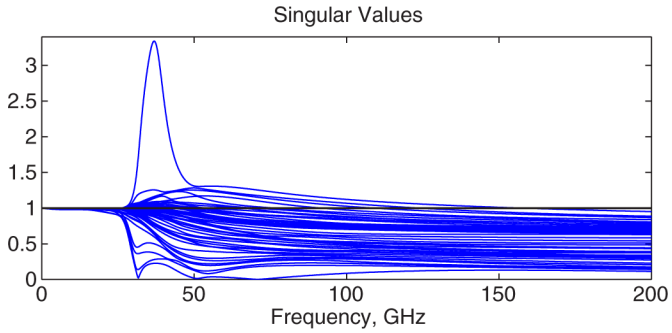

Fig. 15. Singular values of the nonpassive package model of Section V-F. The model was constructed with a hard bound of 0.7 on the asymptotic singular values.

modeled ports over a bandwidth of 5 GHz, for which a macromodel having dynamic order $n = 180$ was derived from frequency-domain scattering responses. The main difficulty with this example is the extended dynamic range of several responses, which must be accurate over a frequency range spanning several decades and starting from 100 Hz. The passivity violations of the original macromodel, depicted in Fig. 12, are moderate in value but located at widely separated frequencies.

Passivity was enforced using SOC and HAM schemes with standard absolute error control, obtaining poor results. Fig. 13 shows significant accuracy degradation where the responses have small magnitude. This level of accuracy is not sufficient to model the isolation level between the various package pins over the required frequency range. This problem was solved using inverse weighting in the definition of the accuracy metric, as described in Section IV. The corresponding results, depicted in Fig. 14, show that both schemes perform equally well.

F. High Complexity Package

The last example we consider is a large QFN package structure with $p = 40$ modeled ports up to 25 GHz. The dynamic order of the macromodel is $n = 400$. This benchmark illustrates the main difficulties that are encountered when the number of modeled ports becomes very large. Although the in-band accuracy can be easily controlled, off-band model behavior may be very poor, as illustrated by the singular value plot of Fig. 15.

As for example Section V-D, the HAM scheme failed to converge due to the nearly singular Hamiltonian matrix resulting from $||\boldsymbol{D}||_2 \simeq 1$. Therefore, a hard constraint on the largest asymptotic singular value was enforced to limit its value to 0.7, resulting in a well-behaved Hamiltonian matrix. Nonetheless, application of standard HAM and SOC schemes led to passivity compensation, with serious accuracy degradation. Figs. 16 and 17 show the behavior of the corresponding passive models on a crosstalk and a transmission response, respectively. An aggressive lowpass filter was necessary to reduce the effects of the off-band model behavior in the accuracy metric, as described in Section IV. The results are depicted in Figs. 18 and 19, showing excellent accuracy even for small responses.

G. Computational Requirements

We now compare the computational requirements of the various passivity enforcement methods, with reference to each analyzed benchmark. Table I summarizes the execution time and

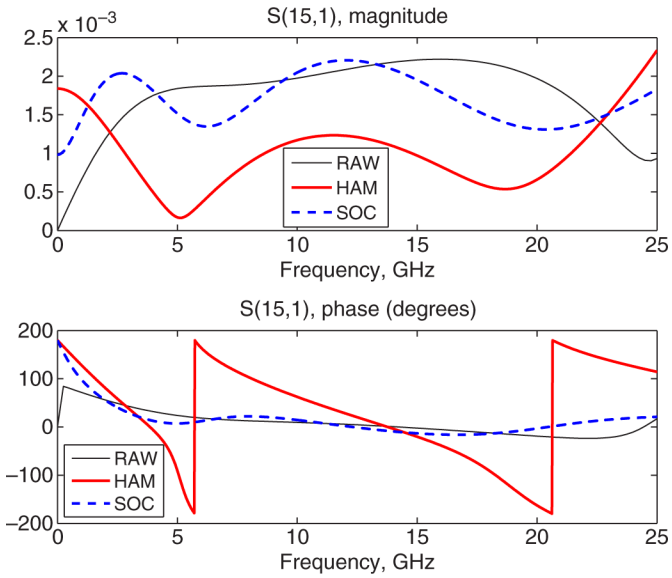

Fig. 16. Crosstalk responses of various passive models compared to raw scattering data for the package structure of Section V-F.

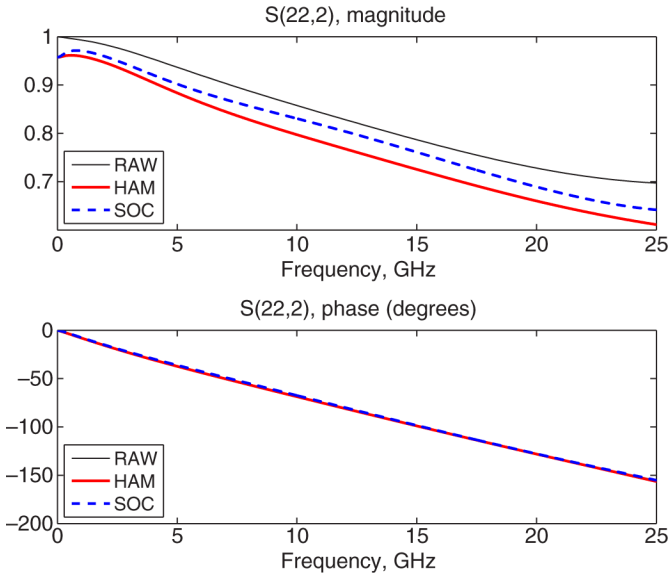

Fig. 17. Transmission responses of various passive models compared to raw scattering data for the package structure of Section V-F.

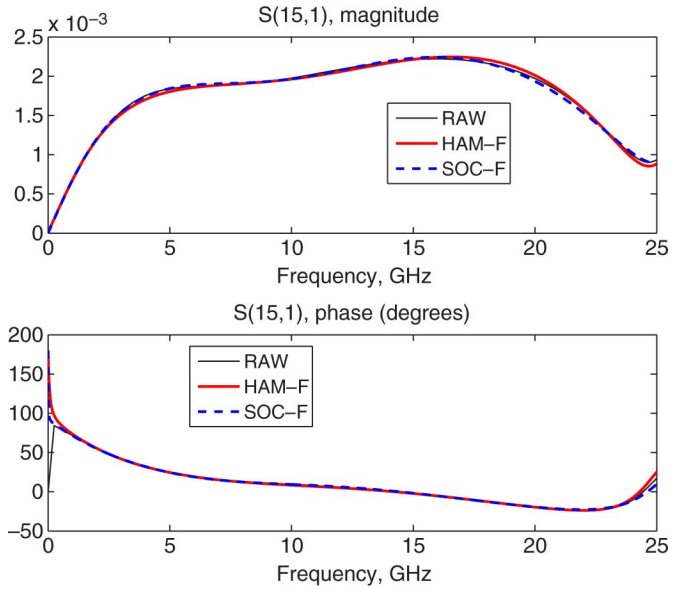

Fig. 18. As in Fig. 16, but employing a lowpass weighted norm during passivity enforcement.

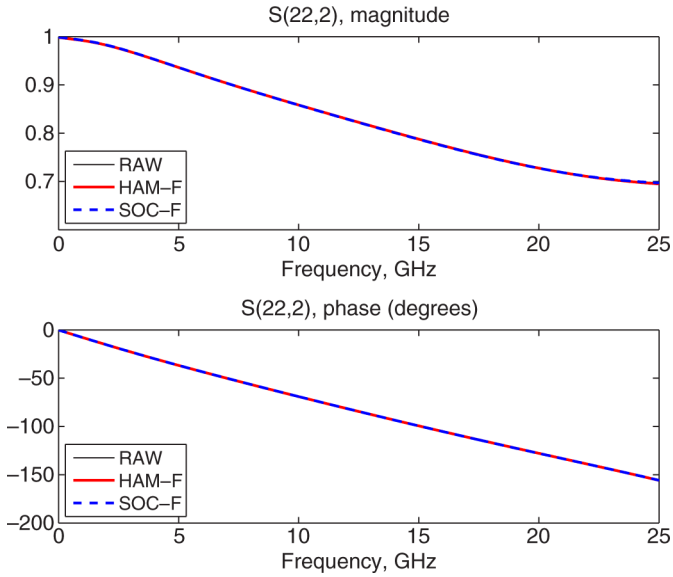

Fig. 19. As in Fig. 17, but employing a lowpass weighted norm during passivity enforcement.

the number of iterations for each case. We remark that these results account for all operations, including adaptive frequency sampling (whenever required) and eigenvalue computation. All obtained macromodels were globally passive. All simulations were run on the same PC with a Pentium IV processor running at 3-GHz clock and with 2 GB of RAM. The table supports the following conclusions.

- BRM and BRD methods are more CPU demanding than HAM and SOC methods and applicable only to low-complexity models. This is readily justified, since the number of BRM/BRD unknowns is $n(n+1)/2+2np$, whereas the number of HAM/SOC unknowns is only np.
- Convergence of SOC is generally faster than HAM in terms of number of iterations.
- SOC requires a larger mean time per iteration than HAM.
- Lowpass weighting (whenever appropriate) improves significantly convergence and CPU time for both HAM and SOC.

In order to support these conclusions on a statistically meaningful set, we deployed an automated process for processing a large number of synthetic examples, parameterized by their dynamic order n and their number of ports p. This process is based on the following steps.

1) Given a prescribed dynamic order n, the macromodel poles are randomly selected with a uniform distribution over the normalized model bandwidth. Each pole has a constant ratio α between real and imaginary part.
2) Residue matrices are also randomly generated and scaled in order to set $\max_\omega ||\boldsymbol{H}(j\omega)||_2 = \beta$, with $\beta > 1$.
3) A total of q independent model realizations are generated for each combination of n and p.

TABLE I
COMPUTATIONAL REQUIREMENTS

Case	Scheme	Iterations	CPU time (s)
V-A	HAM	21	24
V-A	HAM-F	17	14.8
V-A	SOC	5	7.64
V-A	SOC-F	9	6.7
V-A	BRM	16	42.8
V-A	BRM-F	13	33.8
V-A	BRD	22	218
V-B	HAM	18	895
V-B	SOC	5	290
V-C	HAM	34	204
V-C	HAM-F	26	110
V-C	SOC	7	96
V-C	SOC-F	10	78
V-D	SOC	8	78
V-D	SOC-F	6	78
V-D*	HAM	31	191
V-D*	HAM-F	8	148
V-D*	SOC	5	65
V-D*	SOC-F	8	92
V-E	HAM	15	26
V-E	HAM-R	8	15
V-E	SOC	4	13
V-E	SOC-R	4	15
V-F	SOC	8	1217
V-F	SOC-F	10	521
V-F*	HAM	109	3273
V-F*	HAM-F	66	1747
V-F*	SOC	10	1436
V-F*	SOC-F	16	704

* with hard threshold on $\|\boldsymbol{D}\|_2$

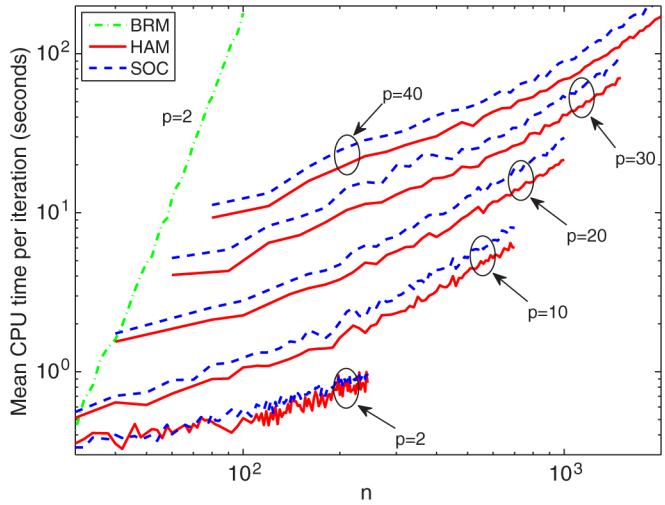

Fig. 20. Mean CPU time per iteration required by different techniques, applied to a statistically significant set of synthetic nonpassive macromodels. See also text.

In all our tests, we used $q = 3$, $\alpha = 1/30$ and $\beta = 1.3$ to insure consistency between all synthetic macromodels when n and p are varied.

Application of BRM, HAM, and SOC schemes leads to the results depicted in Fig. 20. The plot reports the mean CPU time per iteration. As expected, the complexity of BRM prevents its application unless the dynamic order n is very small. The corresponding scaling law with n is approximately n^ν, with $\nu \simeq 5$. Conversely, the scaling law for HAM and SOC has a much more favorable behavior as n^μ, with $\mu \simeq 1$. We can also estimate the scaling with the number of ports p (HAM and SOC only) by keeping n fixed, obtaining p^κ, with $\kappa \simeq 2$. Noting that in our state-space realization each column of the transfer matrix has $n_c = n/p$ poles, the complexity of both HAM and SOC individual iterations can be estimated as $O(n_c p^3)$. Although each SOC iteration is slower with respect to HAM, passivity correction with SOC is generally faster since the number of required iterations is smaller, as confirmed by Table I.

Finally, we remark that data-based accuracy constraints such as (13) are virtually equivalent to using an ideal lowpass filter having infinite off-band attenuation. It is thus expected that such constraints provide the best in-band accuracy when combined with any of the proposed schemes. Unfortunately, the associated computational complexity prevents their use for medium and large-size models. For this reason, we did not implement such constraints with the SOC and HAM schemes, which thus remain the only viable solution for large-scale passive macromodeling, as documented in Section V.

VI. CONCLUSION

This paper presented a thorough comparison between several different classes of passivity enforcement schemes for lumped macromodels. Each scheme has both advantages and disadvantages. In summary, all methods based on BRL/PRL constraints are known to provide the optimal solution, but are only applicable to low-complexity models due to their very large computational requirements, both in terms of memory and CPU time. Suboptimal techniques such as iterative passivity enforcement at discrete frequency samples or global enforcement via perturbation of Hamiltonian matrices are only suboptimal and sometimes fail. However, they are applicable to larger structures, with a favorable scaling with the model complexity. The numerical performance of all techniques in terms of accuracy is dramatically improved when suitable frequency-selective weighting schemes are adopted.

REFERENCES

[1] M. Celik, L. Pileggi, and A. Obadasioglu, *IC Interconnect Analysis*. New York: Kluwer, 2002.
[2] M. Nakhla and R. Achar, "Simulation of high-speed interconnects," *Proc. IEEE*, vol. 89, no. 5, pp. 693–728, May 2001.
[3] B. Gustavsen and A. Semlyen, "Rational approximation of frequency responses by vector fitting," *IEEE Trans. Power Del.*, vol. 14, no. 3, pp. 1052–1061, Jul. 1999.
[4] B. Gustavsen, "Computer code for rational approximation of frequency dependent admittance matrices," *IEEE Trans. Power Del.*, vol. 17, no. 4, pp. 1093–1098, Oct. 2002.
[5] B. Gustavsen and A. Semlyen, "A robust approach for system identification in the frequency domain," *IEEE Trans. Power Del.*, vol. 19, no. 3, pp. 1167–1173, Jul. 2004.
[6] D. Deschrijver and T. Dhaene, "Rational modeling of spectral data using orthonormal vector fitting," in *Proc. 9th IEEE Workshop Signal Propagation Interconnects*, Garmisch-Partenkirchen, Germany, May 10–13, 2005, pp. 111–114.
[7] D. Deschrijver, B. Haegeman, and T. Dhaene, "Orthonormal vector fitting: A robust macromodeling tool for rational approximation of frequency domain responses," *IEEE Trans. Adv. Packag.*, vol. 30, no. 2, pp. 216–225, May 2007.
[8] S. Grivet-Talocia and M. Bandinu, "Improving the convergence of vector fitting in presence of noise," *IEEE Trans. Electromagn. Compat.*, vol. 48, no. 1, pp. 104–120, Feb. 2006.
[9] S. Grivet-Talocia, "Package macromodeling via time-domain vector fitting," *IEEE Microwave Wireless Comp. Lett.*, vol. 13, no. 11, pp. 472–474, Nov. 2003.

[10] VectFit2 [Online]. Available: http://www.energy.sintef.no/produkt/VECTFIT/index.asp
[11] IdEM 2.4 [Online]. Available: http://www.emc.polito.it
[12] V. Belevitch, *Classical Network Theory*. San Francisco, CA: Holden-Day, 1968.
[13] T. Kailath, *Linear Systems*. Englewood Cliffs, NJ: Prentice Hall, 1980.
[14] M. R. Wohlers, *Lumped and Distributed Passive Networks*. New York: Academic, 1969.
[15] S. Boyd, L. El Ghaoui, E. Feron, and V. Balakrishnan, *Linear Matrix Inequalities in System and Control Theory, SIAM Studies in Applied Mathematics*. Philadelphia, PA: SIAM, 1994.
[16] B. D. O. Anderson and S. Vongpanitlerd, *Network Analysis and Synthesis*. Englewood Cliffs, NJ: Prentice-Hall, 1973.
[17] S. Grivet-Talocia and A. Ubolli, "On the generation of large passive macromodels for complex interconnect structures," *IEEE Trans. Adv. Packag.*, vol. 29, no. 1, pp. 39–54, Feb. 2006.
[18] D. Saraswat, R. Achar, and M. Nakhla, "Global passivity enforcement algorithm for macromodels of interconnect subnetworks characterized by tabulated data," *IEEE Trans. VLSI Syst.*, vol. 13, no. 7, pp. 819–832, Jul. 2005.
[19] C. P. Coelho, J. Phillips, and L. M. Silveira, "A convex programming approach for generating guaranteed passive approximations to tabulated frequency-data," *IEEE Trans. Computed-Aided Design of Integr. Circuits Syst.*, vol. 23, no. 2, pp. 293–301, February 2004.
[20] H. Chen and J. Fang, "Enforcing bounded realness of S parameter through trace parameterization," in *Proc. 12th IEEE Topical Meeting Electrical Performance Electron. Packag.*, Princeton, NJ, Oct. 27–29, 2003, pp. 291–294.
[21] B. Dumitrescu, "Parameterization of positive-real transfer functions with fixed poles," *IEEE Trans. Circuits Syst. I, Reg. Papers*, vol. 49, no. 4, pp. 523–526, Apr. 2002.
[22] B. Gustavsen and A. Semlyen, "Enforcing passivity for admittance matrices approximated by rational functions," *IEEE Trans. Power Syst.*, vol. 16, no. 1, pp. 97–104, Feb. 2001.
[23] B. Gustavsen, "Computed code for passivity enforcement of rational macromodels by residue perturbation," *IEEE Trans. Adv. Packag.*, vol. 30, no. 2, pp. 209–215, May 2007.
[24] B. Gustavsen, "Fast passivity enforcement of rational macromodels by perturbation of residue matrix eigenvalues," in *Proc. 11th IEEE Workshop Signal Propagat. Interconnects*, Genova, Italy, May 13–16, 2007, pp. 71–74.
[25] D. Saraswat, R. Achar, and M. Nakhla, "A fast algorithm and practical considerations for passive macromodeling of measured/simulated data," *IEEE Trans. Compon. Packag. Manufact. Technol.*, vol. 27, no. 1, pp. 57–70, Feb. 2004.
[26] S. Grivet-Talocia, "Passivity enforcement via perturbation of Hamiltonian matrices," *IEEE Trans. Circuits Syst. Reg. Papers*, vol. 51, no. 9, pp. 1755–1769, Sep. 2004.
[27] S. Grivet-Talocia, "An adaptive sampling technique for passivity characterization and enforcement of large interconnect macromodels," *IEEE Trans. Adv. Packag.*, vol. 30, no. 2, pp. 226–237, May 2007.
[28] A. Lamecki and M. Mrozowski, "Passive SPICE networks from non-passive data," in *Proc. 16th Int. Conf. Microw., Radar, Wireless Commun. (MIKON)*, Krakóv, Poland, May 22–24, 2006, vol. 3, pp. 981–983.
[29] A. Lamecki and M. Mrozowski, "Equivalent SPICE circuits with guaranteed passivity from nonpassive models," *IEEE Trans. Microwave Theory Tech.*, vol. 55, no. 3, pp. 526–532, Mar. 2007.
[30] S. Grivet-Talocia and A. Ubolli, "On relative error minimization in passivity enforcement schemes," in *Proc. 11th IEEE Workshop Signal Propagation Interconnects*, Ruta di Camogli, Italy, May 13–16, 2007, pp. 75–78.
[31] S. Grivet-Talocia and A. Ubolli, "Passivity enforcement with relative error control," *IEEE Trans. Microwave Theory Tech.*, vol. 55, no. 11, pp. 2374–2383, Nov. 2007.
[32] A. Ubolli and S. Grivet-Talocia, "Weighting strategies for passivity enforcement schemes," presented at the 16th IEEE Topical Meeting Electrical Performance Electronic Packag., Atlanta, GA, Oct. 29–31, 2007.
[33] J. W. Brewer, "Kronecker products and matrix calculus in system theory," *IEEE Trans. Circuits Syst.*, vol. 25, no. 9, pp. 772–781, Sep. 1978.
[34] C. F. Van Loan, "The ubiquitous Kronecker product," *J. Comput. Appl. Math.*, vol. 123, pp. 85–100, 2000.
[35] K. Zhou, J. C. Doyle, and K. Glover, *Robust and Optimal Control*. New York: Prentice Hall, 1996.
[36] S. Boyd and L. Vandenberghe, *Convex Optimization*. Cambridge, U.K.: Cambridge Univ. Press, 2004.
[37] J. F. Sturm, "Using SeDuMi 1.02, a Matlab toolbox for optimization over symmetric cones," *Optimization Methods Software*, pp. 625–653, 1999.
[38] SeDuMi 1.1 [Online]. Available: sedumi.mcmaster.ca
[39] J. Lofberg, "YALMIP: A toolbox for modeling and optimization in MATLAB," presented at the CACSD Conf., Taipei, Taiwan, 2004.
[40] *"Matlab R2007a User's Guide"* [Online]. Available: http://www.mathworks.com
[41] J. H. Wilkinson, *The Algebraic Eigenvalue Problem*. London: Oxford Univ. Press, 1965.
[42] S. Boyd, V. Balakrishnan, and P. Kabamba, "A bisection method for computing the H_∞ norm of a transfer matrix and related problems," *Math. Control Signals Syst.*, vol. 2, pp. 207–219, 1989.
[43] K. Zhou, "Frequency-weighted $\mathcal{L}^\infty$ norm and optimal Hankel norm model reduction," *IEEE Trans. Autom. Control*, vol. 40, no. 10, pp. 1687–1699, Oct. 1995.
[44] X. Chen and K. Zhou, "On the relative and multiplicative model reduction," in *Proc. 27th Southeastern Symp. Syst. Theory*, Mar. 12–14, 1995, pp. 57–60.

Stefano Grivet-Talocia (M'98–SM'07) received the Laurea and the Ph.D. degrees in electronic engineering from the Politechnic University of Turin, Turin, Italy.

From 1994 to 1996, he was with the NASA/Goddard Space Flight Center, Greenbelt, MD, where he worked on applications of fractal geometry and wavelet transform to the analysis and processing of geophysical time series. Currently, he is an Associate Professor of Circuit Theory with the Department of Electronics, the Polytechnic of Turin. His current research interests are in passive macromodeling of lumped and distributed interconnect structures, modeling and simulation of fields, circuits, and their interaction, wavelets, time-frequency transforms, and their applications. He is author of more than 90 journal and conference papers.

Dr. Grivet-Talocia received the IBM Shared University Research (SUR) Award in 2007. He served as Associate Editor for the IEEE TRANSACTIONS ON ELECTROMAGNETIC COMPATIBILITY from 1999 to 2001.

Andrea Ubolli received the Laurea degree in electronic engineering from the Polytechnic of Turin, Turin, Italy, where he is currently working toward the Ph.D. degree.

Since graduation, he joined the EMC Group at the Department of Electronics, Polytechnic of Turin, as a Research Assistant. His research interests are in the field of electromagnetic compatibility, where he works on macromodeling of electrical interconnects and on power integrity in micro- and macroscale complex interconnected systems, with emphasis on passivity enforcement schemes.